MADRID
inter.noise 2019
June 16 - 19
NOISE CONTROL FOR A BETTER ENVIRONMENT

Shallow Water Effects on Ship Underwater Noise Measurements

Sipilä, Tuomas[1]
VTT Technical Research Centre of Finland
Tietotie 1, Espoo; P.O.Box 1000; FI-02044 VTT, Finland

Viitanen, Ville[2]
VTT Technical Research Centre of Finland
Tietotie 1, Espoo; P.O.Box 1000; FI-02044 VTT, Finland

Uosukainen, Seppo[3]
VTT Technical Research Centre of Finland
Tietotie 4C, Espoo; P.O.Box 1000; FI-02044 VTT, Finland

Klose, Rhena[4]
Schiffbau-Versuchsanstalt Potsdam
Marquardter Chaussee 100, 14469 Potsdam, Germany

ABSTRACT

The underwater noise of icebreaker Polaris was measured in shallow water. The measurements were conducted using one hydrophone at the sea bottom and three hydrophones at intermediate depths. The noise measurements were analysed in this paper at port side passes at 11 knots speed. Transmission loss was investigated in shallow water for ranges typical in noise trials between the target ship and the measurement location. The transmission loss at different depths and frequencies was analysed from the measurements. The measured transmission loss was compared to the results of acoustic propagation models. The sensitivity of transmission loss to bathymetry and seabed sediment characteristics was studied numerically by systematically varying bottom geometry and its acoustic properties. The noise measurements conducted with two different methods gave relatively close results although the measurements were done in water depths not reaching the minimum levels of classification notations. The numerical simulations revealed the complicated underwater acoustic environment present in shallow waters.

Keywords: Underwater noise, Ship, Shallow water
I-INCE Classification of Subject Number: 14

[1] tuomas.sipila@vtt.fi
[2] ville.viitanen@vtt.fi
[3] seppo.uosukainen@vtt.fi
[4] klose@sva-potsdam.de

1. INTRODUCTION

Underwater noise emitted from shipping has become a concern due to increased environmental awareness. There is rising pressure to restrain the acoustic footprint of shipping. The adverse effects of shipping noise on marine mammals became of concern in the 1970s when the overlap between the main frequencies used by large baleen whales and the dominant components of noise from ships was noted [1]. The fish have also been observed to be disturbed by ship emitted noise [2].

In naval and research vessels, the sound emitted from a ship or a submarine can interfere with the measurement equipment, or the acoustic footprint can be used for detection.

International attention has been put to the underwater noise topics. The EU Marine Directive (MSFD 2008/56/EC) aims to achieve Good Environmental Status (GES) of the EU's waters by the year 2020. The subcommittee of IMO on ship design and equipment (DE) established a correspondence group on minimizing underwater noise [3]. The correspondence group has developed non-mandatory guidelines for reducing underwater noise from commercial ships. Canada organized a wide international workshop "Quieting Ships to Protect the Marine Environment" in IMO in January 2019.

To determine the underwater noise levels of a ship, field tests are conducted where the noise level is measured utilizing a specific method. The underwater noise is measured using hydrophones when the ship is passing the measurement point at a specified speed. Classification societies have different requirements for the measuring techniques regarding the number of hydrophones used and their depths, distance between the measurement point and the vessel, etc.

The noise level of a ship is determined as a source level of a singular monopole source (SL) at one meter distance from the source. The radiated noise level (RNL) of a vessel is calculated from the background noise corrected sound pressure level (SPL') at the hydrophone by

$$RNL = SPL' + X \log_{10}\left(\frac{r}{r_0}\right) \qquad 1$$

where X is a geometrical parameter, r is the range between the vessel and the measurement location, and r_0 is the reference distance ($r_0 = 1$ m). The latter term on the right hand side of Equation 1 represents the geometrical transmission loss in water. For spherical propagation in unbounded medium the parameter $X = 20$ dB, and for cylindrical propagation, e.g. in shallow water environment, the parameter $X = 10$ dB. Based on practical experience, alternative figures for the parameter X are presented such as $X = 18$ dB in the DNV Silent Class Notation [4] and $X = 19$ dB in the BV rule note for Underwater Radiated Noise for shallow water [5]. Source level is calculated from the radiated noise level by making corrections due to sound absorption and reflections from the sea surface and bottom. In the DNV method, the surface correction is neglected.

This paper investigates the geometrical transmission loss factor X in underwater noise measurements conducted for icebreaker Polaris in late autumn 2016 in the coastal waters of Helsinki. The measurements were done in ice-free conditions in shallow water. VTT and SVA Potsdam conducted the measurements in co-operation. The sensitivity of transmission loss on the bottom geometry and sediment properties was demonstrated with a propagation model. Section 2 describes the noise measurements conducted for Polaris and the propagation model used in the investigation. The results of the measurements are shown in Section 3, as well as the transmission loss predicted by the numerical propagation model. The conclusions are given in Section 4 and the acknowledgements in Section 5.

2. METHODS

2.1 Noise Measurements

The vessel under test was the icebreaker Polaris. She is built in Arctech Helsinki Shipyard in 2016, and owned and operated by Arctia. The vessel fulfils the polar class PC4. The maximum speed of the vessel is 17 kn in open water. The main engines are equipped with dual fuel capability for LNG and marine diesel oil, and during the measurements, MDO was used. The ship consists of two 6.5 MW Azipod units at the stern and one 6.0 MW Azipod unit at the bow. During the tests, only the after Azipod propellers were run while the fore Azipod propeller was windmilling. Main dimensions and characteristics of the vessel are given in Table 1. A photograph of the vessel during the measurements is shown in Figure 1.

The underwater noise from the ship was measured multiple times at speeds of 6 and 11 knots. For this paper, only the measurements made from the port side of the vessel at 11 knots speed are analysed. The cavitation inception speed is slightly exceeded at 11 knots speed.

Table 1. Main characteristics of IB Polaris.

Length	110 m
Beam	24 m
Draught	8 m
Displacement	10 961 tons
Maximum speed	17 kn
Engine	2 x Wärtsilä 9L34DF
	2 x Wärtsilä 12V34DF
Propulsion	2 x ABB Azipod 6.5 MW at stern
	1 x ABB Azipod 6.0 MW at bow

Figure 1. A photograph of the IB Polaris during the noise measurements.

The wave height was between 0.3-0.4 m during the measurement day based on the observations made on board Polaris and the measurement boat. Wind speed of 6-8 m/s was recorded by the measurement system of Polaris. The wind direction was from the north, and consequently the fetch was very short in the measurement site.

As discussed earlier in this paper, the measurements were conducted in shallow water. The measurements took place on a silent seaway. The water depth at the Polaris measurement route was about 25 - 27 meters. The water depth does not meet any class notation limitations to the minimum water depth. The measurement boat was located above a slope in the seabed. The water depth at the location of the measurement boat was about 21 meters. The bottom type is complex in the measurement area. It compounds of

rock, mixed sediments and clay. The bottom types in the measurement region are shown in Figure 2.

The sound speed profile in the water column at the location of the measurement boat was determined from the measured temperature and density distributions. The sound speed profile in the water column was uniform being $c_w = 1447.7$ m/s.

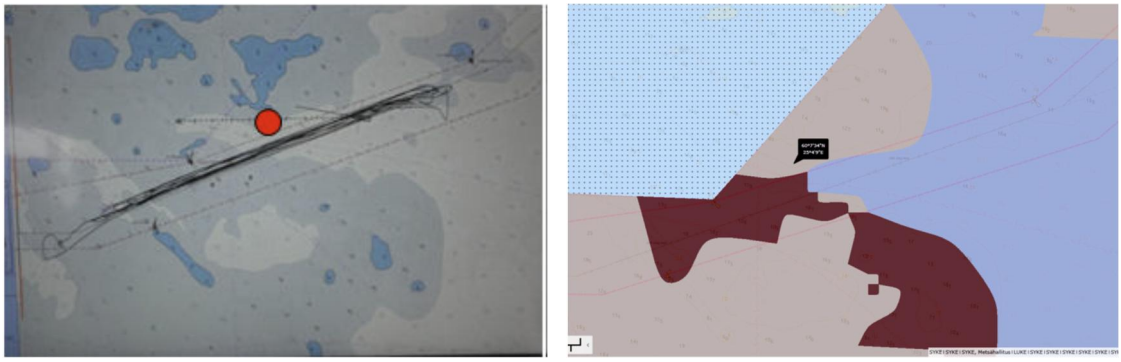

Figure 2. The measurement area. On the left: Polaris route during the measurements. The measurement boat location is indicated by the red circle; On the right: Sea bottom sediment type. Blue color denotes clay, light red color denotes mixed sediments, and dark red color denotes rock. Location of the measurement boat is indicated. The seaway limits are indicated with dashed pink lines in both figures.

The measurement setup is sketched in Figure 3. The measurement boat is anchored to the side of the path of the ship under test. In the figure, the hydrophone in the seabed cage and the three-hydrophone array configuration are shown. The hydrophone cage is similar to that shown in DNV class notations [5]. The cage was submerged to a depth of 21 m. The hydrophones on the three-hydrophone array were submerged to depths of 6 m, 8 m and 10 m.

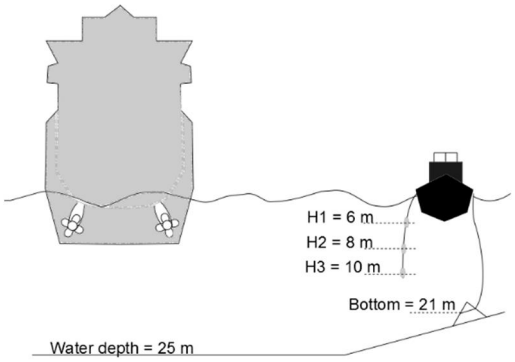

Figure 3. A sketch of the measurement setup.

VTT measured underwater noise from the seabed with Brüel & Kjær 8106 hydrophone and the measurement data is recorded with LMS Scadas III data acquisition system and LMS Test.Lab software. The sampling frequency is 208 kHz. The entire measurement system is checked at the beginning and end of the measurements with Brüel & Kjær 4229 hydrophone calibrator. SVA Potsdam performed underwater noise measurements with three hydrophones in intermediate depths in the water column. The hydrophones were submerged to 6 m, 8 m and 10 m depths. The hydrophones were equipped with a sinker such that they did not move in the current. The measurement equipment consisted of three ELAC-Nautic KE9 hydrophones and the measuring system PAK-MKII from Müller BBM for data acquisition and further processing. The sampling frequency for each hydrophone was 100 kHz. The calibration of the measurement chain

was conducted with a Brüel & Kjær 4223 hydrophone calibrator. The VTT and SVA measuring systems were supplied by batteries.

The measurement manoeuvre of the vessel under test is shown schematically in Figure 4. The measurement boat is anchored at a side of the measurement route of the vessel. The vessel under test passes the measurement boat at the prescribed speed on a straight course with constant machinery setting, and the distance to closest point of approach d_{cpa} is determined. The target passing distance in each measurement leg is $150\text{ m} \leq d_{cpa} \leq 250\text{ m}$ following the recommendations of DNV class notations [4]. The underwater noise measurement is initiated when the bow of the vessel reaches closest point of approach. Accoding to DNV class notifications [4], the data window length (DWL) for the measurements above 5 knots speed is twice the ship length as shown in Figure 4. The passing distance in each analysed measurement leg is shown in Table 2, as well the propulsion power and rotational rate of the stern propellers.

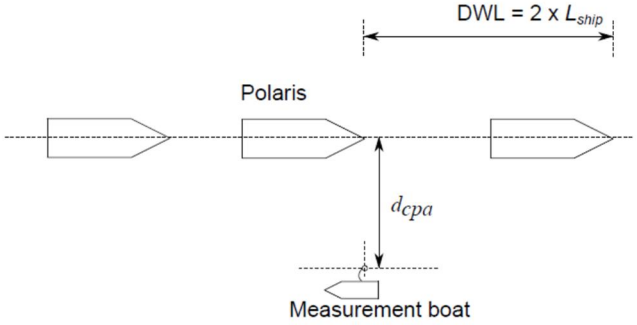

Figure 4. A sketch of Polaris passing the measurement point.

Table 2. List of analysed measurements and the related parameters for analyses.

Test	Ship speed [kn]	Side	Passing distance d_{cpa} [m]	Azipod, port side Power [kW]	Azipod, port side propeller. rpm	Azipod, starboard side Power [kW]	Azipod, starboard side propeller. rpm
# 10	11.3	PS	173	1734	139	1643	138
# 12	11.2	PS	174	1742	138	1697	139
# 14	11.2	PS	163	1608	137	1589	136
# 16	11.3	PS	136	1653	137	1585	137

From the hydrophone measured pressures p, sound pressure level L_p in dB is defined as $L_p = 20\log_{10}\frac{p_{rms}}{p_{ref}}$, where p_{rms} is the root-mean-square of the measured pressure signal and the reference pressure in water is $p_{ref} = 1\mu\text{Pa}$. The measured sound pressure levels are checked against the background noise levels at each 1/3 octave band.

2.2 Propagation Model

Several noise propagation models have been developed for modelling range independent (depth-dependent only) or dependent propagation of sound at low and high frequencies. Etter [6,7] has ranked the propagation models based on their capability to predict low or high frequency noise in deep or shallow waters, and their practicality from the simulation time point of view. The maximum water depth for shallow water is considered as 200 m and the threshold frequency for low/high frequency noise is 500 Hz. A range dependent parabolic equation model RAM [10] was used in this study for low and moderate frequency noise modelling. The open source code RAM available in Ocean Acoustic Library (OAL) [11].

The elliptic wave equation can be expressed in frequency domain in cylindrical coordinates in axial symmetry case as [8]

$$\frac{\partial^2 q}{\partial r^2} + k^2 \frac{\partial}{\partial z}\left(\frac{1}{k^2}\frac{\partial q}{\partial z}\right) + k^2 q = 0 \qquad 2$$
$$q = p\sqrt{r}$$

where r is the range in cylindrical coordinates, z is the depth, q is a sound pressure related quantity, p is the sound pressure, and k is the wave number.

The axial symmetry arises from a line source excitation which may be a Gaussian field or a normal mode solution. The equation above does not hold at $r = 0$ (excitation line).

It is assumed that the variable q can be expressed as

$$q(r,z) = \Psi(r,z)e^{-jk_0 r} \qquad 3$$

If parameter k is assumed as a slowly varying function of depth z and Ψ is a slowly varying function of range r according to the narrow angle approximation,

$$\frac{\partial}{\partial z}\left(\frac{1}{k^2}\right) \approx 0$$
$$\left|\frac{\partial^2 \Psi}{\partial r^2}\right| \ll \left|2k_0 \frac{\partial \Psi}{\partial r}\right| \qquad 4$$

a parabolic partial differential equations PDE for Ψ is obtained [9]

$$-2jk_0 \frac{\partial \Psi}{\partial r} + \frac{\partial^2 \Psi}{\partial z^2} + (k^2 - k_0^2)\Psi = 0 \qquad 5$$

This can be solved by marching r with the finite difference method. The marching begins from $r = 0$ where the starting field $\Psi(0,z) = q(0,z)$ is defined.

Equation 5 can be extended to wider elevation angles by substituting it with the expression [9]

$$\frac{\partial \Psi}{\partial r} + jk_0\left(\sqrt{\left(\frac{k}{k_0}\right)^2 + \frac{1}{k_0^2}\frac{\partial^2}{\partial z^2}} - 1\right)\Psi = 0 \qquad 6$$

where negligible backscattering and weak range dependence of k are assumed. Equation 6 can also be expressed as

$$\frac{\partial \Psi}{\partial r} + jk_0(Q-1)\Psi = 0$$
$$Q = \sqrt{1+q}, \quad q = \varepsilon + \mu \qquad 7$$
$$\varepsilon = \left(\frac{k}{k_0}\right)^2 - 1, \quad \mu = \frac{1}{k_0^2}\frac{\partial^2}{\partial z^2}$$

The equation above can be solved utilizing a Taylor series of Q but the second order terms of q complicates the numerical implementation [9]. The square root term can be presented as Padé approximation, i.e., a rational-function presentation so that its value and derivatives to the highest possible orders agrees with the corresponding terms of the square root at $q = 0$. The Padé approximation can be presented in form [9]

$$\sqrt{1+q} = 1 + \sum_{j=1}^{m} \frac{a_{j,m} q}{1 + b_{j,m} q} \qquad 8$$

Padé series provide the highest accuracy in the main propagation direction but cause some phase errors between propagation angles [9].

The operator Q in Equation 7 can be splitted as

$$Q = \sqrt{1+\mu} + \sqrt{1+\varepsilon} - 1 \qquad 9$$

The parabolic wave equation can be solved by the efficient split-step Fourier algorithm by using this expression. By solving Equation 7 one obtains

$$\Psi(r+\Delta r) = \Psi(r) e^{-jk_0 \Delta r(\sqrt{1+q}-1)} \quad 10$$

Applying Padé approximation in Equation 8 to Equation 10, one obtains

$$e^{-jk_0 \Delta r(\sqrt{1+q}-1)} \simeq 1 + \sum_{j=1}^{m} \frac{a_{j,m} q}{1 + b_{j,m} q} \quad 11$$

Equations 10 and 11 form the split-step Padé solution devised by Collins [10]. The solution is valid for problems involving very wide propagation angles, large depth variations and elastic sea bottoms. According to Collins, the solution is as accurate as higher-order parabolic equation solutions and approximately two orders of magnitude faster than the other finite difference solutions of parabolic equations.

3. RESULTS

3.1 Noise measurements

Figure 5 shows the measured source level of IB Polaris at 1/3 octave band at 11 knots speed as measured from the bottom hydrophone and from the three hydrophones in intermediated depths. Also, the power average of the radiated noise level of the three hydrophones is shown. The DNV Silent-E (transit) class limit for vessel underwater noise is given in the figure for reference. The measurement data is post-processed according to the DNV class notations [4], i.e., the distance correction and bottom reflections are taken into account. Corrections due to reflections from the water surface are not done.

It is seen that the noise level of IB Polaris is below the Silent-E (transit) limit over the whole noise spectrum. The noise level at $f_c = 800$ Hz center frequency slightly exceeds the limit when measured with the hydrophones at the intermediate depths but with the bottom hydrophone, the noise level is below the limit also at that central frequency. The bottom hydrophone measures higher sound pressure levels at low frequencies, whereas the sound pressure levels above about $f_c > 80$ Hz are higher in the intermediate depths. Narrowband analysis of the sound pressure levels, which is not shown here, reveals that the highest sound pressure levels are caused by stern propeller tip vortex cavitation and electric motors of the propulsion units.

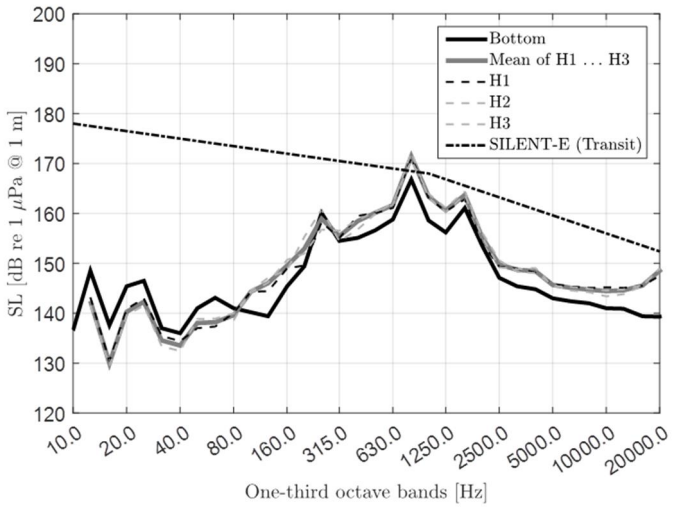

Figure 5. The measured sound pressure levels in 1/3 octave bands for the ship speed of 11 knots measured with different hydrophones.

3.2 Transmission loss in shallow water

Figure 6 shows uncorrected sound pressure levels at 1/3 octave band at central frequencies $f_c = 63$, 630, 1000, and 1250 Hz at the bottom hydrophone and at the three hydrophones at the intermediate depths. In addition, the power averaged values of the hydrophones are also given the figure. The measured sound pressure levels are given for 11 knots speed for the different test runs. The distance between the IB Polaris and the measurement point varies somewhat between the test runs as can be seen from the figure and Table 2. The abscissas in Figure 6, representing non-dimensional distance d_{cpa}/r_0, are given in logarithmic scale. As a result, the slope between the different measurements runs at the same hydrophones represent the overall transmission loss factor X_{oa}, similar to Equation 1 where the geometrical transmission loss is presented.

For the bottom hydrophone, the slopes seem to increase gradually from $X_{oa} \approx 10$ dB at $f_c = 63$ Hz to $X_{oa} \approx 15$ dB at $f_c = 1250$ Hz. The hydrophones at the intermediate depths give similar slopes as the bottom hydrophone at the lowest frequency $f_c = 63$ Hz. At higher frequencies, the slopes at the intermediate depths seem to be very mild or even ascending.

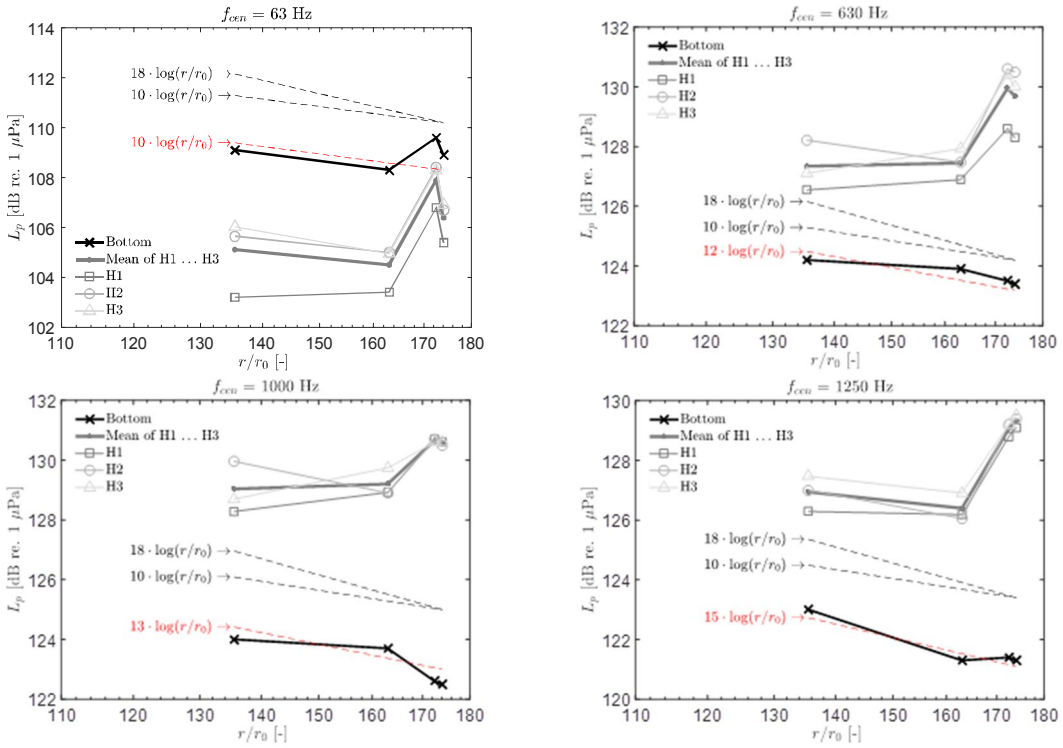

Figure 6. Uncorrected sound pressure levels at the bottom hydrophone and hydrophones at intermediate depths for test runs 10, 12, 14, and 16 with varying portside passing distances. The results are given for central frequencies $f_c = 63$, 630, 1000, and 1250 Hz at 1/3 octave band.

3.3 Noise propagation modelling

The transmission loss simulations were conducted with the actual bottom geometry and sediment type, and celerity profile. The point source was set to the depth of the 0.7 propeller radius when the blade is pointing upwards. The results are analysed normal to the ship route in the water and the bottom sediment. The transition loss was analysed more carefully at the depths of the hydrophones used in the measurements. The simulations were conducted using gravel as the bottom sediment type.

The sensitivity of transmission loss to the bottom sediment type and bottom geometry are also studied. The geoacoustic properties of the investigated bottom sediment

types are given in Table 3, where ρ_b/ρ_w is the ratio of the densities in bottom and water, c_b is the sound speed in bottom, and α_b is the attenuation in bottom as dB per wavelength λ.

Table 3. Geoacoustic properties of bottom sediment types [12].

Bottom type	ρ_b/ρ_w	c_b [m/s]	α_b [dB/λ]
Gravel	2.0	1800	0.6
Moraine	2.1	1950	0.4
Sand	1.9	1650	0.8
Clay	1.5	1500	0.2

Figure 7 shows transmission loss at a cross-sectional area normal to the ship route at the closest point of approach. A green line in the figure, as well as in Figures 9 and 10 draws the sea bottom. The source is located in these figures at the right-hand side at depth 4.13 m and the hydrophone locations are illustrated by turquoise circles. The transmission loss is given in water and bottom sediment at $f = 63$ and 630 Hz. The horizontal distributions of the transmission loss at the depths of the hydrophones used in the measurements are also given in the figure. It is seen that the transmission loss is complicated in shallow water. Acoustic energy proceeds into the bottom sediment especially at lower frequencies. The surface and bottom reflections make the transmission loss complex in the underwater environment, especially at higher frequencies.

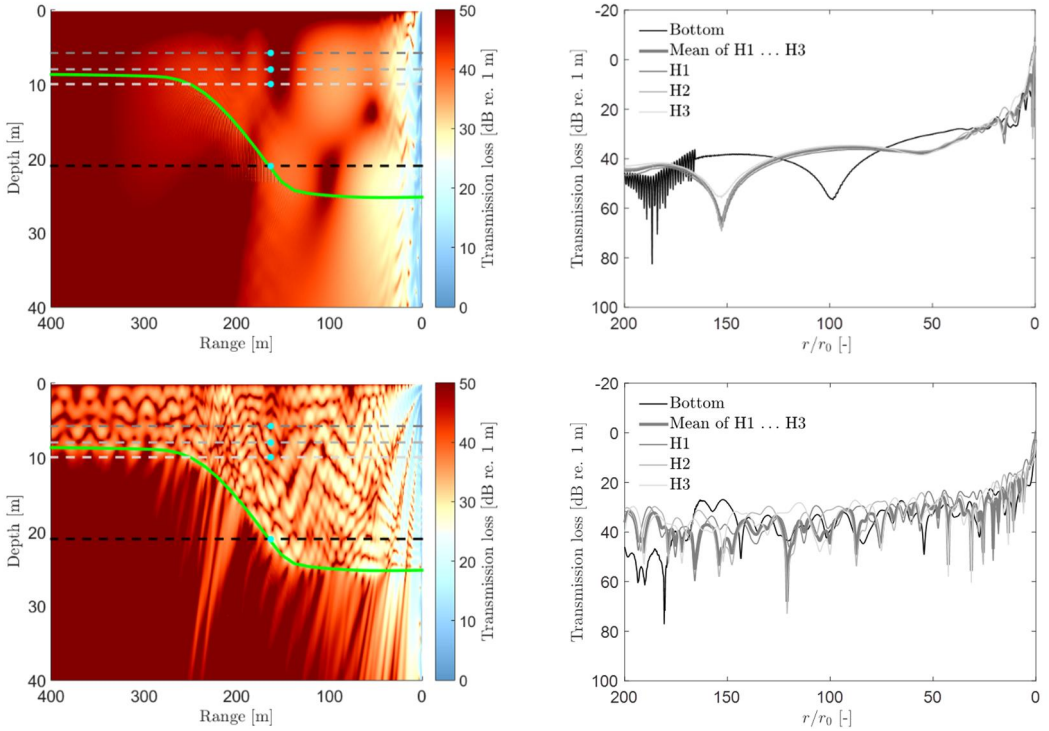

Figure 7. Modelled transmission loss. At left: transmission loss in the cross-sectional area normal to ship route at the closest point of approach. At right: transmission loss along horizontal lines at the depths of the hydrophones. At top $f = 63$ Hz; at bottom $f = 630$ Hz.

Figure 8 presents the slope of the overall transmission loss X_{oa} determined from the measured sound pressure levels at the bottom hydrophones and simulations over a wide range of frequencies. The slopes from the measurements are determined from 1/3 octave band analyses whereas the simulation results are analysed from narrow band

analyses. The measurement results refer to those presented in Figure 6. The slopes from the analyses were determined from data between 100 and 160 meters.

The slopes analysed from the measured and simulated results have have similar magnitude. It is seen that the slope distributions fluctuate a lot but the trend shows increasing transmission loss towards higher frequencies both in the measurements and in the analyses.

The sensitivity of the transmission loss on the bottom sediment properties is investigated in Figure 9. The transmission loss at a cross-sectional area normal to the ship route is shown with clay sediment at frequency $f = 630$ Hz. Compared to the similar simulation with gravel sediment in Figure 7, it is seen that more acoustic energy passes to the bottom with clay sediment. Consequently, the transmission loss is higher with the clay sediment. In general, the transmission loss is affected by the bottom sediment type up to 10 dB at the bottom hydrophone at a range of about 160 meters from the source.

Figure 10 shows the sensitivity of the transmission loss on the bottom geometry. The slope of the bottom is varied so that the depth of the bottom hydrophone as well as the depth under the vessel are kept the same but the slope of the bottom is varied as illustrated in Figure 10. The transmission loss at a cross-sectional area normal to the ship route is shown with gravel sediment at frequency $f = 630$ Hz for the mildest slope. Comparison to other bottom slopes shows that the transmission loss is not very sensitive to the bottom geometry in this case.

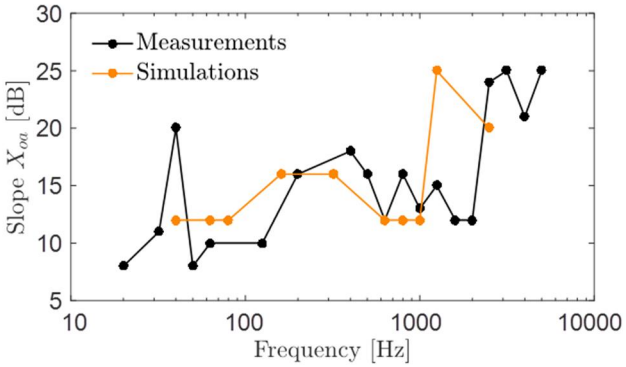

Figure 8. Overall measured and simulated transmission loss slope at different frequencies at the bottom hydrophone.

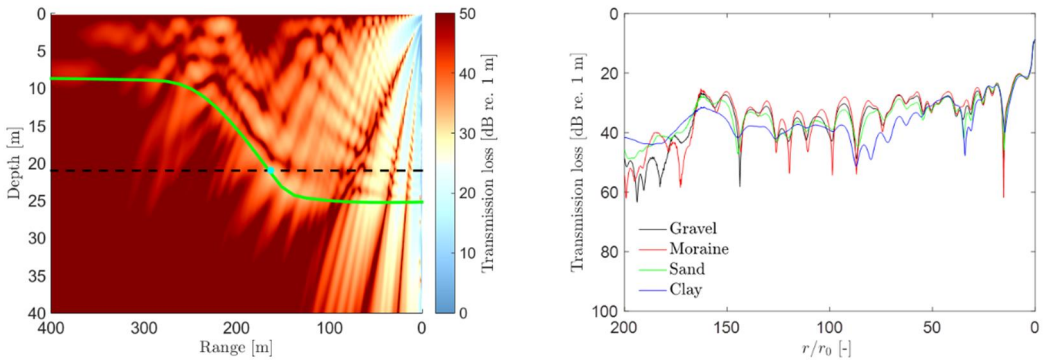

Figure 9. Noise transmission loss with different bottom sediment types at the frequency $f = 630$ Hz. At left: transmission loss in the cross-sectional area normal to the ship route at the closest point of approach. The bottom sediment is clay. At right: transmission loss along the horizontal line at the depth of the bottom hydrophone for different bottom sediment types.

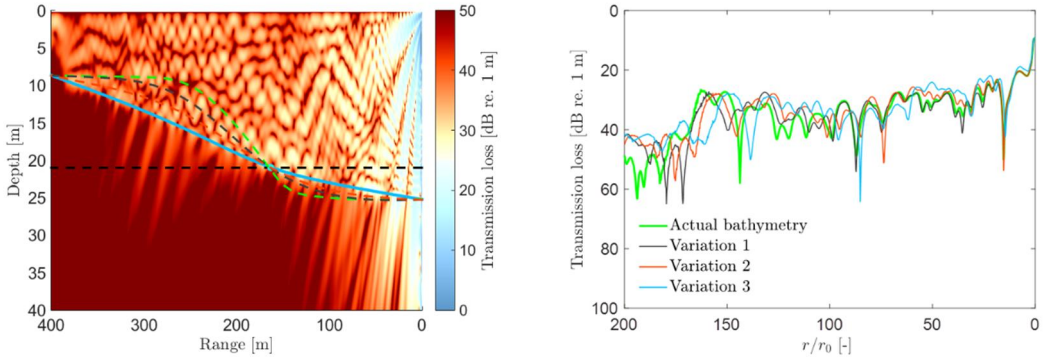

Figure 10. Noise transmission loss with different bottom sediment types at the frequency $f = 630$ Hz. At left: transmission loss in the cross-sectional area normal to the ship route at the closest point of approach. The transmission loss is drawn for the lowest bottom slope. At right: transmission loss along the horizontal line at the depth of the bottom hydrophone with different bottom slopes.

4. CONCLUSIONS

Underwater noise of Polaris was measured near Helsinki shoreline in late autumn 2016. The measurements were conducted in shallow water. The effect of shallow water on the noise propagation was investigated using measured and simulated transmission loss data. This paper concentrated on the analyses of the results from the port side passes at 11 knots speed.

The acoustic source level of IB Polaris was measured with a bottom hydrophone and with three hydrophones at intermediate depths. The two measurement methods gave rather similar results. At lower frequencies, the bottom hydrophone gave higher sound pressure levels than the hydrophones at intermediate depths. At higher frequencies, the measured sound pressure levels were vice versa. One can speculate that at lower frequencies the first mode of a standing acoustic wave forms in the water column and increases the sound pressure at the bottom. The simulated transmission loss also shows lower levels near the bottom compared to that at intermediate depths at low frequencies.

The range of variations between the ship and the measurement point were too small to determine the frequency dependent transmission loss reliably. The reflections from the surface and the bottom complicate the transmission loss pattern in water significantly as can be seen from the analyses. However, the measured and simulated transmission loss levels were similar and showed an increasing trend towards higher frequencies.

The sensitivity analyses made from the simulations showed that the bottom sediment types have up to 10 dB influence on the transmission loss levels even at the investigated short distances. The transmission loss seemed to be less sensitive to the bottom geometry variations in the present case although the influence of geometry alterations are clearly visible in the figures.

5. ACKNOWLEDGEMENTS

The authors want to express their gratitude to Arctia for providing the icebreaker Polaris for the underwater noise measurements. The authors are grateful to the Finnish Navy for assisting in planning and executing the noise measurements, and providing the Jurmo landing craft to carry out the measurements. The authors are grateful for ABB Marine and Ports for giving the propulsion data for the analyses of the measurements and for the inspiring discussions. The work was done in PropNoise project funded by Tekes

– the Finnish Funding Agency for Innovation under the research programme Arctic Seas and German Federal Ministry for Economic Affairs and Energy.

6. REFERENCES

1. R.S. Payne and D. Webb. "*Orientation by means of long-range acoustic signaling in baleen whales*". In H. E. Adler, editor, Orientation: Sensory basis. Ann. N.Y. Acad. Sci., (1971)
2. R.B. Mitson. "*Underwater noise from research vessels - review and recommendations*". Cooperative Research Report No. 209, International Council for the Exploration of the Sea, (1995)
3. IMO, "*Guidelines for the reduction of underwater noise from commercial shipping to address adverse impacts on marine life*", MEPC.1/Circ.833 (2014)
4. DNV, "*Silent Class Notation*" Rules for classification of Ships, Part 6 Chapter 24 (2010)
5. Bureau Veritas, "*Underwater Radiated Noise (URN)*", Rule Note NR614 DT R00 E (2014)
6. P.C. Etter, *"Underwater Acoustic Modeling and Simulations"* 3rd ed., Spon Press, London (2003)
7. P.C. Etter, "*Review of Ocean-Acoustic Models*", Oceans (2009)
8. E.M. Salomons, *"Computational Atmospheric Acoustics"* Kluver Academic Publishers, Dordrecht (2001)
9. F.B. Jensen, W.A. Kuperman, M.B. Porter and H. Schmidt, *"Computational Ocean Acoustics"*, Springer (2011)
10. M.D. Collins, *"A split-step Padé solution for the parabolic equation method"* J. Acoust. Soc. Am. 93(4), Pt.1, (1993)
11. http://oalib.hlsresearch.com/ (26.2.2019)
12. L.M. Brekhovskikh, Y.P. Lysanov, "*Fundamentals of Ocean Acoustics*", Springer-Verlag, New York (2002)